A hydrogeomorphic dataset for characterizing catchment hydrological behavior across the Tibetan Plateau

Yuhan Guo[1], Hongxing Zheng[2], Yuting Yang[1], Yanfang Sang[3], Congcong Wen[4,5]

[1]State Key Laboratory of Hydroscience and Engineering, Department of Hydraulic Engineering, Tsinghua University, Beijing, 100101, China
[2]CSIRO Environment, Canberra, ACT 2601, Australia
[3]Key Laboratory of Water Cycle and Related Land Surface Processes, Institute of Geographic Sciences and Natural Resources Research, CAS, Beijing, 100101, China
[4]NYUAD Center for Artificial Intelligence and Robotics, New York University Abu Dhabi, UAE
[5]NYU Tandon School of Engineering, New York University, USA

Correspondence to: hongxing.zheng@csiro.au

Abstract

Hydrologic and geomorphic processes are intricately linked within the Earth system, jointly characterizing terrestrial hydrological behaviors and biogeochemical cycles across diverse temporal and spatial scales. The Tibetan Plateau provides an ideal setting for investigating the interactions between hydrological and geomorphic processes in a largely pristine natural environment. Nonetheless, the interactions remain largely unknown due to challenging physical conditions and data limitations. This study presents the inaugural version of a hydrogeomorphic dataset encompassing 18,440 catchments across the region. The dataset comprises 18 hydrogeomorphic metrics, particularly along with the width function and width function-based instantaneous unit hydrograph (WFIUH) of each catchment. We find that the peak flow of WFIUH is positively related to slope and curvature but negatively related to catchment area, perimeter, length, and circularity. The relationships of time-to-peak against the hydrogeomorphic metrics are similar to those of peak flow but in an oppositive direction. Catchment concentration time shows a positive relationship with catchment size but a strong negative correlation with catchment slope. The validity of the derived WFIUH has been confirmed by its successful integration into an hourly hydrological model for simulating flash flood events. Uncertainties in the WFIUH can be attributed to the resolution of DEM and the methods employed for calculating flow velocity. The dataset is publicly available via the Zenodo portal: https://doi.org/10.5281/zenodo.8280786 (Guo and Zheng, 2023). It can contribute to advancing our understanding of catchment hydrological behaviors and providing simple and fast routing unit hydrograph calculation for ungauged catchments in the Tibetan Plateau, and hence improve water resources management and disaster mitigation in the region and its downstream.

1 Introduction

Hydrologic and geomorphic processes are intricately linked within the Earth system, jointly characterizing terrestrial hydrological processes and biogeochemical cycles across diverse temporal and spatial scales. The interactions between these processes play a critical role in governing water flow, shaping landforms, and influencing sediment and nutrient transportation within ecosystems (Babar, 2005; Scheidegger, 1973; Sidle and Onda, 2004). The exploration of the interactions can be traced back to Horton's foundational contributions (Horton, 1945) and the classical works of Strahler (1957), Kirkby (1976) and Rodríguez-Iturbe and Valdés (1979). Since then, extensive endeavors have been undertaken in hydrology and geomorphology to investigate the hydrologic behavior of a catchment in response to its geomorphic attributes (Jenson, 1991).

Hydrogeomorphologic data consisting of various geomorphic attributes (e.g., slope, elevation, curvature, and catchment shape attributes) has demonstrated value in predicting hydrological behavior for ungauged basins (Esper Angillieri, 2008), mapping flood-prone zones (Lindersson et al., 2021) and determining the groundwater potential zones. On top of the morphologic or topographic metrics describing catchment properties, the geomorphologic instantaneous unit hydrograph (GIUH) introduced by Rodríguez-Iturbe and Valdes (1979) is of utmost interest for hydrologists to derive hydrograph in the absence of hydrologic data (Bhaskar et al., 1997; Jain et al., 2000; Nasri et al., 2004; Nowicka and Soczynska, 1989; Kumar et al., 2007). The concept of GIUH was extended by Gupta et al. (1980) to theoretically deduce the unit hydrograph based on geomorphology, topographic parameters, and hydrographic parameters. The GIUH assumes that the probability distribution of the water droplet travel time is exponential, which however lacks practical physical meaning (Gupta and Waymire, 1983; Kirshen and Bras, 1983; Rinaldo et al., 1991). The assumption is arguable and it is also challenging to determine flow velocity while deriving GIUH (Rodríguez-Iturbe and Valdes, 1979; Troutman and Karlinger, 1985). An alternative geomorphology-based unit hydrograph is based on the geomorphic width function (Kirkby, 1976). The width function is commonly considered as one of the most important geomorphologic and hydrologic features quantifying the influence of the river network on catchment hydrologic processes (Mesa and Mifflin, 1986; Naden, 1992), which determines the shape of the instantaneous unit hydrograph (Botter and Rinaldo, 2003). Franchini and O'connell (1996) compared WFIUH against GIUH and suggested that WFIUH is more physically consistent and more practical.

The Tibetan Plateau is known as the water tower of Asia, supplying water to almost 2 billion people (Yao et al., 2012; Li et al., 2022; Mtamba et al., 2015). Hydrogeomorphic characteristics of catchments within the Tibetan Plateau are unique and with little human intervention (Yao et al., 2022; Mölg et al., 2014). The geographical uniqueness of the Tibetan Plateau provides ideal opportunities to explore the interactions between hydrologic and geomorphic processes. However, hydrogeomorphic data of catchments across the Tibetan Plateau are still limited for a systematic investigation of the hydrogeomorphic process in the region. Particularly, the Tibetan Plateau is experiencing more extreme precipitation events and floods (Ge et al., 2019; Yang et al., 2022), which makes it imperative to develop a comprehensive hydrogeomorphic dataset to inform flood modeling and adaptive watershed management.

This research aims to provide an inaugural version of the hydrogeomorphic dataset for catchments over the Tibetan Plateau. The dataset includes 18 hydrogeomorphic measurements of 18440 catchments within the plateau, which are derived from a high-resolution digital elevation model (DEM) or compiled from existing products. Most importantly and uniquely, the research provides the first dataset of WFIUH for each catchment, which can be used to investigate the spatial heterogeneity of hydrological behavior across the Tibetan Plateau. The derived WFIUH are tested and validated as applied to flood modeling for gauged catchments. This dataset is expected to contribute to a better understanding of hydrogeomorphic processes and to facilitate hydrological modeling of catchments across the Tibetan Plateau.

2 Study area and data

The Tibetan Plateau (TP) is situated between 26°~~00~~ to 40°N and 73° to 105°E and has a mean elevation of more than 4500 meters, occupying about 2.5 × 10^6 km². TP is the highest and most extensive highland in the world. In addition to having the largest cryospheric extent outside the polar region, the TP also serves as the source region for all major rivers in Asia. Consequently, it has been widely acknowledged as the driving force behind both regional and global environmental change (Kang et al., 2010). The Mekong River, the Yellow River, the Yangtze River, the Yarlung Tsampo (Brahmaputra), the Indus and the Karnali all originate on the Tibetan plateau and support hundreds of millions of people downstream. Due to the harsh and complex natural environment, the Tibetan Plateau is a typical ungauged area in China. Within the boundary of China, the Tibetan Plateau can be roughly divided into several basins, namely the Inland region basin, the Yellow River basin, the Yangtze River basin, and the Southwest basin (Figure 1).

In this study, the hydrogeomorphic dataset we developed covers 18440 catchments across the Tibetan Plateau. The boundaries of the catchments are determined according to the HydroBASINS dataset, where the 12th level catchments are considered (https://www.hydrosheds.org/products/hydrobasins). ~~In deriving the width function for each catchment,~~In deriving the width function for each catchment from the digital elevation model (DEM), it needs to produce the flow direction raster map first. The Tibetan Plateau has numerous endorheic basins (mainly in the inland region in Figure 1), and the algorithms applied to determine flow directions of endorheic and exorheic basins can be slightly different (e.g., Prusevich et al. (2022). As this study does not focus on the algorithms determining flow direction but mainly on generating the WFIUH for flash flood modeling, we use the flow direction raster map from HydroSHEDS (https://www.hydrosheds.org/hydrosheds-core-downloads~~)~~ ~~is also used,~~), which ~~based~~bases on DEM from NASA's Shuttle Radar Topography Mission (SRTM) with spatial resolution around 90m (Lehner et al., 2008).

Land cover data product FROM-GLC (Finer Resolution Observation and Monitoring-Global Land Cover）released by Peng Gong et al. (2019) is used in this study to estimate the Manning coefficient in calculating flow velocity. The spatial resolution of the land cover data is 10m. It is resampled by the bilinear approach to be consistent with the flow direction map. For hydrological modeling validity, hourly rainfall and streamflow data of 4 hydrological stations are obtained from China's Annual Hydrological Report. Boundaries of the 18440 catchments and locations of the hydrological stations are shown in Figure 1.

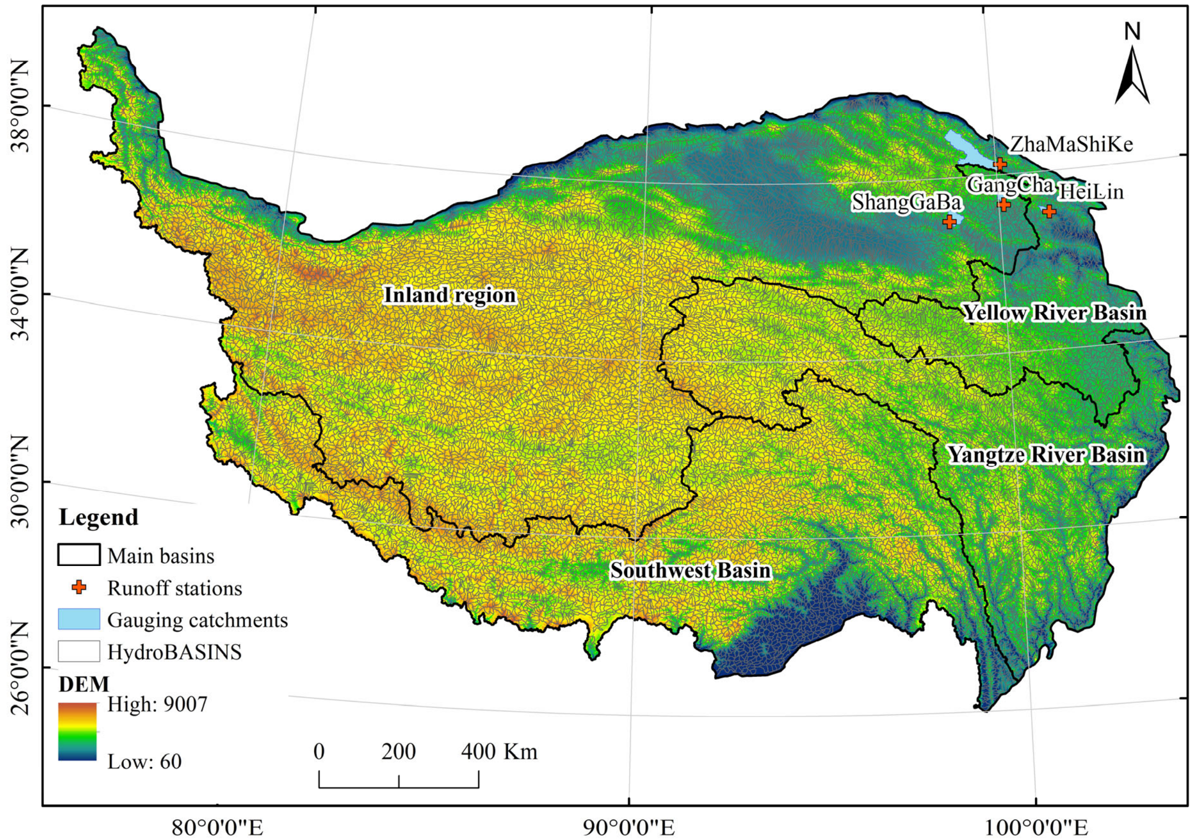

Figure 1 Elevation and boundaries of 18440 HydroBASINs catchments across the Tibetan Plateau

3 Methods

The overall framework for producing the hydrogeomorphic dataset for catchments over the Tibetan Plateau is shown in Figure 2. The framework mainly consists of three procedures, i.e., extracting critical hydrogeomorphic metrics from DEM or existing data products, deriving width function for catchments based on terrain analysis, and generating WFIUH for all catchments. The derived WFIUH is then tested by incorporating it into a hydrological model to simulate hydrological processes at a catchment scale.

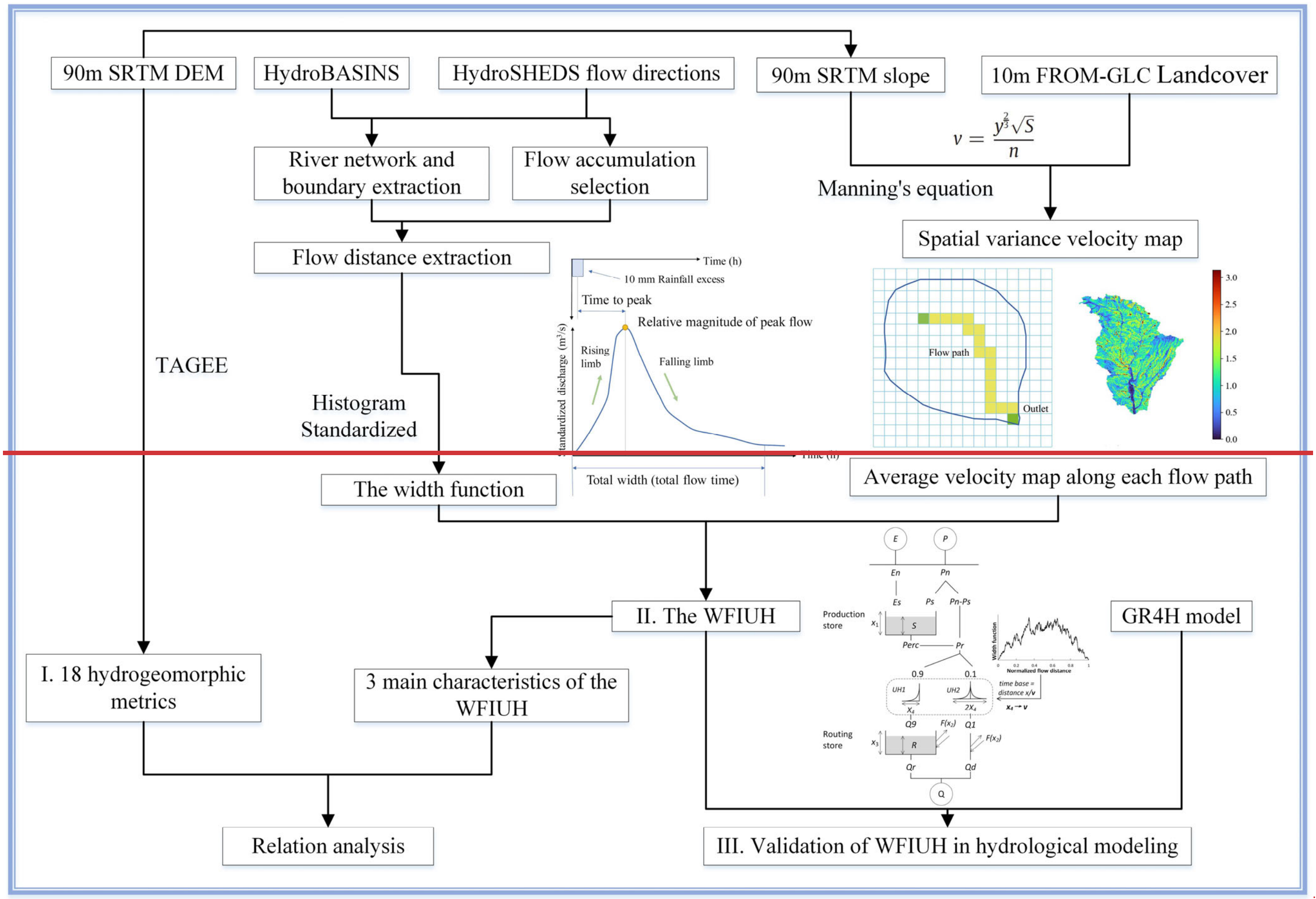
90m SRTM DEM
HydroBASINS
HydroSHEDS flow directions
90m SRTM slope
10m FROM-GLC Landcover
River network and boundary extraction
Flow accumulation selection
$v = \frac{y^{\frac{2}{3}}\sqrt{S}}{n}$
Manning's equation
Spatial variance velocity map
Flow distance extraction
Time (h)
10 mm Rainfall excess
Time to peak
Relative magnitude of peak flow
Rising limb
Falling limb
Flow path
Outlet
TAGEE
Histogram Standardized
The width function
Total width (total flow time)
Average velocity map along each flow path
II. The WFIUH
GR4H model
I. 18 hydrogeomorphic metrics
3 main characteristics of the WFIUH
Relation analysis
III. Validation of WFIUH in hydrological modeling

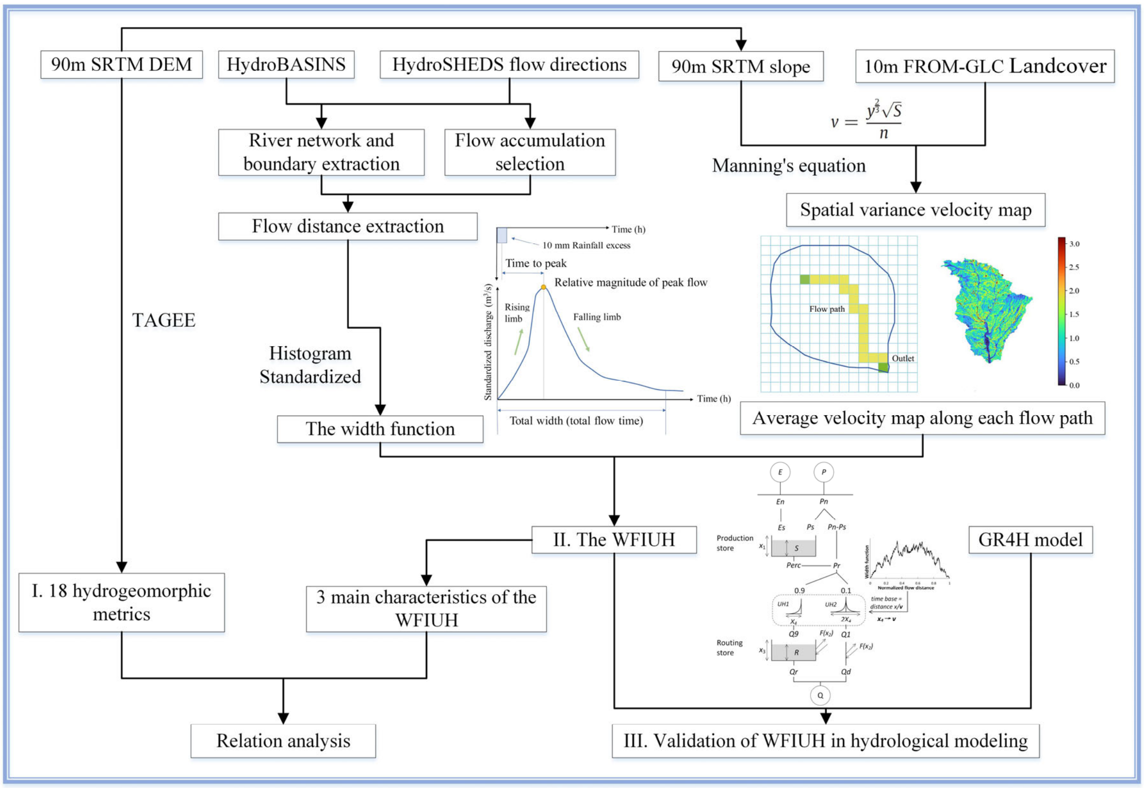

Figure 2 Framework of developing catchment-scale hydrogeomorphic dataset of the Tibetan Plateau

3.1 Catchment-scale hydrogeomorphic metrics

In this dataset, 18 hydrogeomorphic metrics at a catchment scale are retrieved from DEM or compiled from existing datasets. The hydrogeomorphic metrics are closely related to hydrologic and geomorphic processes for the catchments, including area, consisting of area, the longitude of centroid, latitude of centroid, mean elevation, slope, aspect, northness, eastness, perimeter, catchment length, catchment width, elongation, circularity index, form factor, shape index, Gaussian curvature, hillshade, horizontal curvature and vertical curvature. Definitions of each metric are shown in Table 1.

Several topographic and geomorphic attributes are gained from a package called Terrain Analysis in Google Earth Engine (TAGEE) (Safanelli et al., 2020) using Google Earth Engine platforms. The curvature shows the complexity of the undulation of the ground and it is a quantitative measure of curvature degree and change-point on the terrain surface. The horizontal curvature indicates the degree of curvature and change of the surface along the horizontal direction, which could affect the convergence and dispersion of water flow. The vertical curvature is the degree of elevation change along the maximum slope of the ground slope, which could affect the speed of water flow, resulting in different erosion or accumulation rates. Mean curvature and the Gaussian curvature both characterize the comprehensive curvature features. According to Safanelli et al. (2020), Northness and Eastness can be derived from the aspect. The aspect and derived products, such as Northness and

Eastness attributes, can be linked to the potential solar irradiation on terrain. Mathematical expressions of these metrics listed in Table 1 can be referred to Florinsky (2016). It is worth noting that the shape index (SI) is a continuous numerical form of Gaussian landform classification proposed by Koenderink and Van Doorn (1992). The range of the shape index is -1 to 1. When the value is negative, the surface is concave, and if the value is positive, the surface is convex. When the absolute value of the shape index is within 0.5-1.0, the surface is elliptical. When the absolute value of the shape index is within 0-0.5, the surface is hyperbolic. The shape index expression is as follows:

$$SI = \frac{2}{\pi} arctan \frac{H}{\sqrt{H^2 - K}} \quad (1)$$

In the formula, H and K are parameters used to characterize the shape of the surface (such as ridge or valley, convex or concave). For illumination of the datasets, the expressions of circularity index (CI), form factor (Rf), elongation ratio (Re) and are presented respectively herein:

$$CI = \frac{A_{\text{catchment}}}{A_{circle}} \quad (2)$$

$$R_f = \frac{A_{catchment}}{L_{catchment}{}^2} \quad (3)$$

$$R_e = \frac{L_{circle}}{L_{catchment}} \quad (4)$$

where, $A_{\text{catchment}}$, $L_{catchment}$ are the area and length of a catchment. A_{circle} is the area of a circle whose perimeter equals the watershed's perimeter. L_{circle} is the diameter of a circle that equals the catchment area. The circularity index represents the ratio of the catchment area to the area of a circle with an equivalent perimeter. It ranges between 0 and 1. The catchment is closer to a circular shape for a higher CI value. The Form factor is the ratio of catchment area to squared catchment length. A higher Rf indicates a closer fan-shaped catchment. The Elongation ratio is the ratio of L_{circle} to catchment length. A smaller value of Re reflects a more elongated catchment.

Metrics such as area, perimeter, catchment length, catchment width, elongation ratio, circularity index, and form factor are retrieved from HydroBASINS sub-catchment shapes. The elevation and slope metrics are derived from SRTM DEM with a spatial resolution of around 90m. Before retrieving the metrics for the Tibetan Plateau domain, all the maps have been reprojected to the same coordination system.

Table 1 Descriptions of 18 hydrogeomorphic metrics provided in TPHGD dataset

Metrics	Descriptions	Units
Area	Area of catchment	km^2
Perimeter	Perimeter of catchment	km
Catchment length	Straight distance from the outlet to the farthest point in a catchment	km
Catchment width	The narrowest distance perpendicular to the line between the outlet and the farthest point	km
Elevation	The mean elevation of the catchment	meter
Slope	Mean slope of the catchment	degree

Aspect	Compass direction	degree
Northness	Degree to north	N/A
Eastness	Degree to east	N/A
Circularity index	see formula **2**	N/A
Form factor	see formula **3**	N/A
Elongation ratio	see formula **4**	N/A
Shape index	~~Continuous~~The continuous form of Gaussian landform classification, see formula **1**	N/A
Hillshade	Brightness of illuminated terrain	N/A
Horizontal curvature	Curvature tangent to the contour line	meter
Vertical curvature	Curvature tangent to slope line	meter
Gaussian curvature	Product of maximal and minimal curvatures	meter
Mean curvature	Mean of horizontal and vertical curvatures	meter

3.2 Width function from DEM

The width function (WF) of a catchment is more informative than a single hydrogeomorphic metric in reflecting runoff response to catchment landforms. The width function is defined as the probability measure at a given distance x to the outlet of the i_{th} link measured along with the river network (Rinaldo et al., 1995). With the assumption that every water drop in the channel network travels to the outlet at the same velocity, mathematically, the width function W(x) is expressed:

$$W(x) = \sum_{i=1}^{n} b(x; x_i^u, x_i^d) \quad (5)$$

where n is the number of links in the network, x_i^u and x_i^d are the distances of the upstream and downstream ends of link i from the outlet, and the function b(x) is expressed as:

$$b(x; x_i^u, x_i^d) = \begin{cases} 1, & x_i^d \leq x < x_i^u \\ 0, & \text{otherwise} \end{cases} \quad (6)$$

Integrated along the longest flow path, the relationship between the catchment area and the width function can then be expressed as (Moussa, 2008):

$$Area = \int_0^{L_{max}} W(x)dx \quad (7)$$

Therefore, for comparison among different catchments, the width function can be normalized as:

$$W'(x^*) = W(x)/Area, \ with\ x^* = x/L_{max} \quad (8)$$

In this study, we develop the width function for each catchment based on the flow direction map from HydroSHEDS by using the *pysheds* package in Python (https://github.com/mdbartos/pysheds). Given the flow direction map, catchment delineation and river network extraction proceeded after the implementation of flow accumulation. The threshold of flow accumulation is set to be the 96th percentile of the total accumulation as an easy and efficient way compared with other more complex methods (Passalacqua et al., 2010). Based on the derived river network, the flow distance of each DEM grid is computed and the width function is estimated as the histogram of the catchment area (represented by the number of grids) against flow distance.

3.3 Width function-based instantaneous unit hydrograph

The width function is closely related to the development of a geomorphic instantaneous unit hydrograph (Singh et al., 2014). The WF-based IUH (i.e., WFIUH) is the combination of the WF with any possible linear routing scheme. If only river network routing is taken into account, the convection-diffusion equation can be applied to calculate the WFIUH after stream network ordering (Franchini and Oconnell, 1996). The expression form of WFIUH becomes the following form:

$$WFIUH(t) = \int_0^{L_{max}} f_x(t)W(x)dx \tag{9}$$

where, $f_x(t)$ represents the flow time distribution at the distance x along the river network in a watershed and $W(x)$ is the width function. L_{max} is the largest length of the stream network.

Equation 9 ignores hillslope routing within a catchment. The hillslope routing however could be a critical process in determining runoff response to rainfall and shaping the IUH (Saco and Kumar, 2004). With the consideration of the effects of hillslope routing, it is proposed to combine the spatial distribution of flow velocity and the width function to derive WFIUH (Grimaldi et al. (2010), which is adopted in this study. Four approaches are commonly used to calculate flow velocity (Grimaldi et al., 2010), including Darcy–Weisbach's formula (Katz et al., 1995), Manning's formula, the Soil Conservation Service (SCS) formula (Haan et al., 1994), and the uniform flow formula (Maidment et al. (1996). Making use of a remotely sensed land cover dataset, we herein adopt Manning's formula in our calculation, which is expressed as:

$$v = \frac{y^{\frac{2}{3}}\sqrt{S}}{n} \tag{10}$$

where, n is Manning's roughness coefficient that is related to the land cover type of catchments, and its unit is $m^{-\frac{1}{3}}s$.

To calculate the velocity, as shown in Figure 2, a spatial map of the slope for each catchment is produced based on DEM from SRTM. The 10m FROM-GLC landcover data is then resampled to 90m resolution to match with that of DEM. Manning's roughness n for each 90m grid was assigned according to the look-up table of land cover type against roughness (Table S1 in Supplementary).

4 Results

4.1 Spatial distribution of hydrogeomorphic characteristics

Eighteen hydrogeomorphic metrics of 18440 catchments across the Tibetan Plateau are provided in our dataset (TPHGD). Metrics of a small portion of catchments (<1%) are missing due to spatial mismatch or data quality. Figure 3 presents a statistical summary of the metrics, while Figure 4 shows spatial patterns of the metrics across the Tibetan Plateau. As shown in Figure 3, the area of the 18440 catchments ranges between 4.8 km^2 and 216 km^2, with the perimeter that varies from 9.8 km to 132.7 km and catchment mean elevation between 123.8m to 6180.9m. Most of the catchments are located between 2200m and 6100m. Catchments with higher elevations are in the western and central parts of the TP. Catchments in the western and southeast TP are steeper than other catchments in the TP. Catchment length and width are similar in their statistical distribution (Figure 3), both largely between 1-30km.

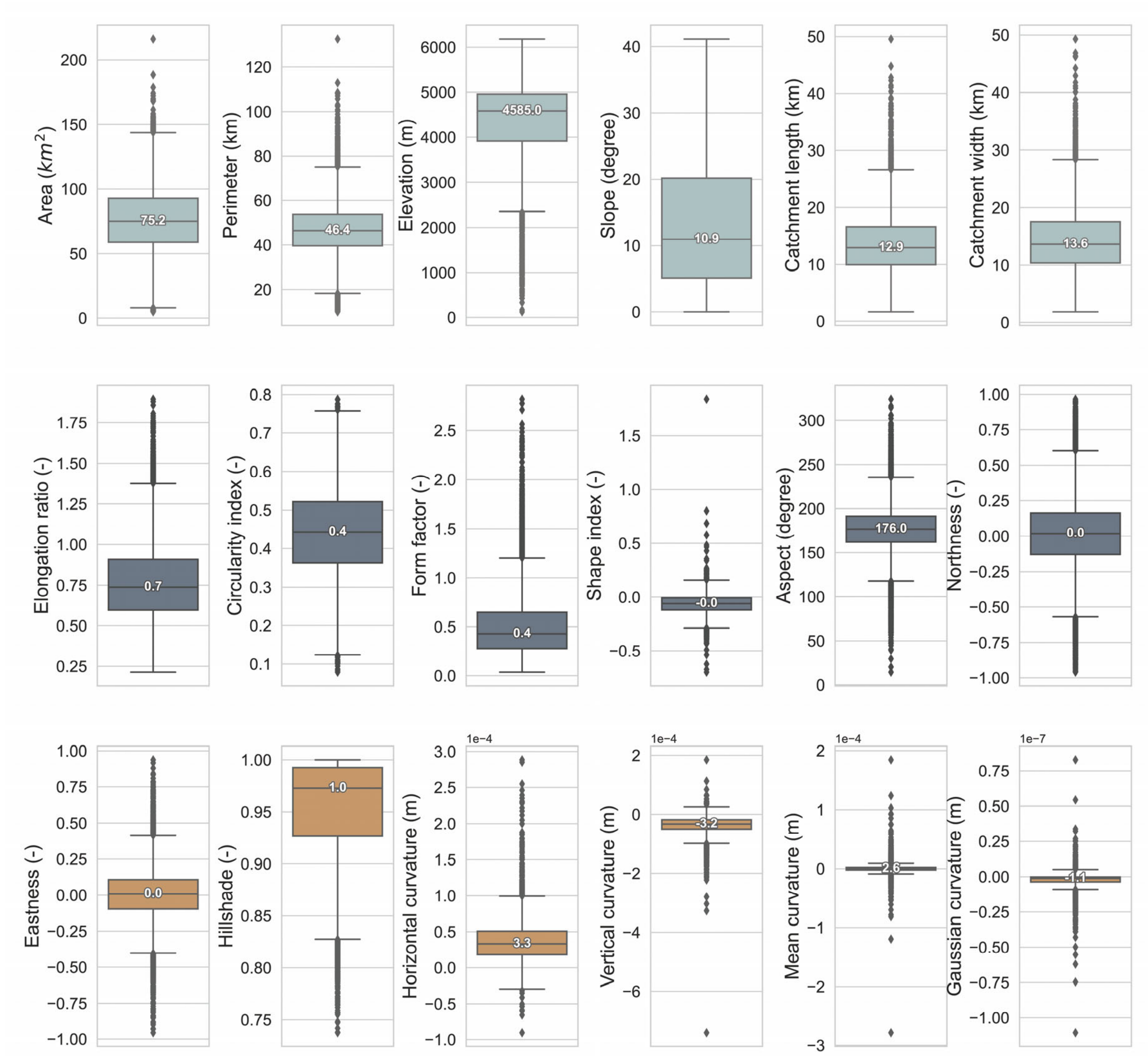

Figure 3 Statistical summaries of 18 hydrogeomorphic metrics for 18440 catchments across the Tibetan Plateau.

Ranges of the elongation ratio, circularity index, and form factor of the catchments are 0.2-1.9, 0.08-0.79, and 0.04-2.82 respectively. Around three-quarters of the catchments have an elongation ratio lower than 1, which means the majority of catchments tend to be elongated. Catchments in central TP are more elongated (Re>1.0) and are with a pinnate river network (Rf>1.0). Catchments located in western and eastern TP are less elongated and more fan-shaped (Figure 4). Most catchments show concave hyperbolic land surface, with a shape index between -0.5 and 0, except for catchments located in the southeast TP. Most catchment aspects are between 150 and 200 degrees with their northness and eastness ranging between -0.25-0.25

and -0.5-0.5 respectively. This reveals that most catchments in TP face southwest, south, or southeast. ~~Hillshade~~The hillshade of most catchments is above 0.9 (Figure 3). Catchments in southeast TP have lower hillshade, suggesting that they are in the alpine and valley areas with a higher shading effect. The curvature of a catchment affects the movement of water, sediment and biogeochemical matters. In addition to the horizontal and vertical curvatures, the Gaussian and mean curvatures for each catchment are recorded in our dataset as well. The median horizontal and vertical curvatures of all the TP catchments are around 0.33×10^{-3} m and -0.32×10^{-3} m respectively. Medians of mean and Gaussian curvature are 0.26×10^{-3}m and -0.11×10^{-6} m respectively. It is worth noting that the curvature metrics in our dataset represent that at a catchment scale, which are averages of each grid cell within the catchment. Hence, catchments with less curvature suggest a greater extent of flat or plain terrain within the catchment.

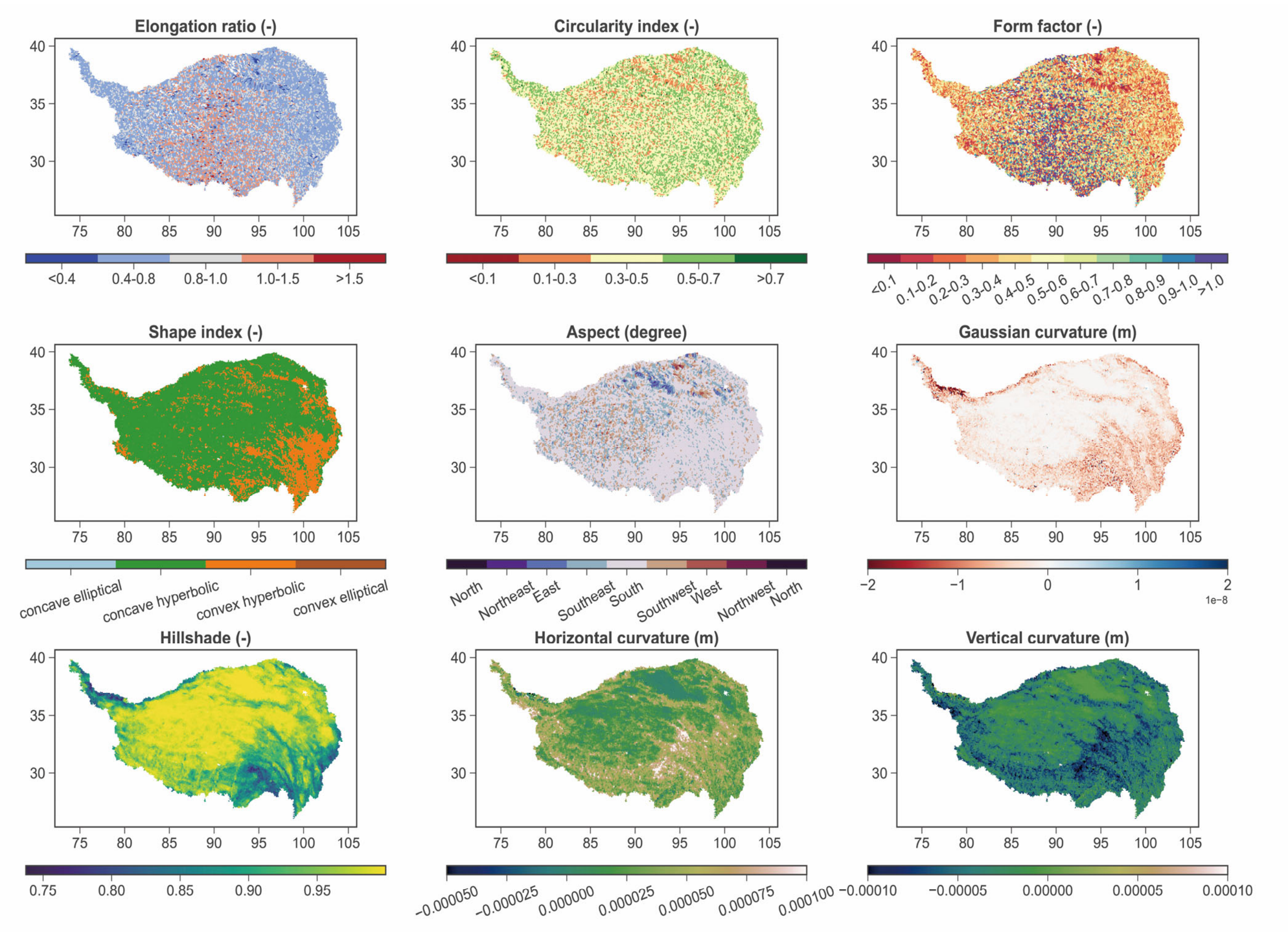

Figure 4 Spatial patterns of hydrogeomorphic metrics across the Tibet Plateau

Figure 5 shows correlations among the 18 metrics. Catchment area (Ac) is found significantly correlated with catchment length (Lc), width (Lw), and perimeter (Pc), and could be represented by the power law (Figure 5(b), (c), (d)). The relationship between Ac and Lc largely follows Hack's law (Rigon et al., 1996; Sassolas-Serrayet et al., 2018), which suggests a power law between the length of the river channel and the drainage area. The catchment perimeter is negatively correlated with the circularity index (with a correlation coefficient r=-0.55). Elongation ratio, circularity index, and form factor are highly related to catchment length, catchment width, and perimeter as can be expected according to Eqs.2-4. The form factor and the elongation ratio are highly related (r=0.98). This may indicate that the elongation ratio and form index represent similar shape information of a catchment. The slope of the catchments is correlated negatively with hillshade (r=-0.97), vertical curvature (r=-0.49) and Gaussian curvature (r=-0.53), but positively with shape index (r=0.36) and horizontal curvature (r=0.52). There is no significant correlation between catchment slope and elevation with a correlation coefficient of no more than ±0.3.

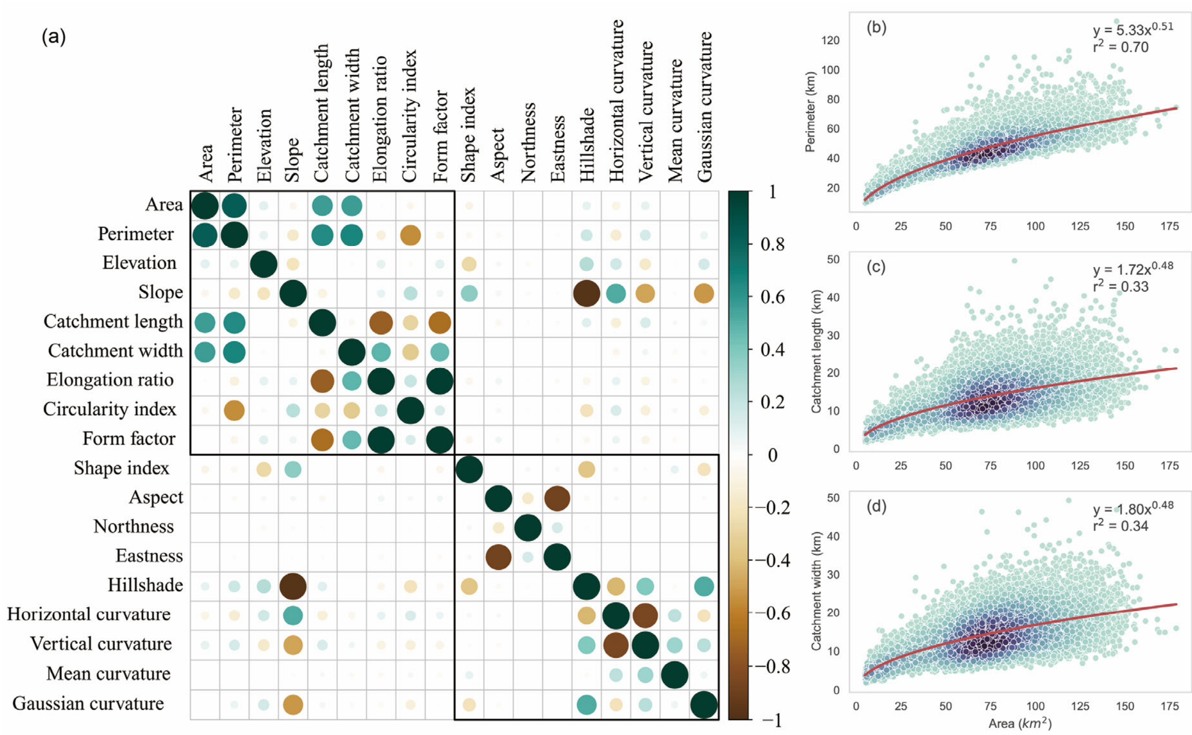

Figure 5 Correlation between the 18 hydrogeomorphic metrics (left) and relationships between catchment area against catchment length, width and perimeter (right).

4.2 Classification of catchment's width function

The width function of a catchment is a comprehensive curve reflecting the effects of landform on hydrological behavior and is used to develop the instantaneous unit hydrograph for catchments across the TP. In TPHGD, normalized width functions of 13,456 out of the 18,440 catchments are presented since it is less meaningful to derive the width function of a catchment with a relatively smaller area. The normalized width functions of the 13,456 catchments across the TP are grouped into five types by using the K-means unsupervised clustering approach and the Gap Statistic method.

Shapes of the five types of width functions are shown in Figure 6. The first two types of width function both have a notable peak value in the curve (i.e., area proportion against distance to catchment outlet). However, the WF_I is peak-centered while WF_{II} is peak-skewed. The shape of catchments characterized by these two types of width functions is typically elongated, with tributaries predominantly located in the upstream areas, resulting in relatively lengthy routing pathways. The third type of the width function (WF_{III}) is largely uniform-like without notable peaks. This width function type is often observed in catchments with larger overall areas or with a relatively consistent density of river networks extending from upstream to downstream. The fourth (WF_{IV}) and fifth (WF_V) types of width function are with dual peaks. The main difference between them is that the first peak in WF_{IV} is dominant, while the two peaks in WF_V are much closer values. Catchments with WF_{IV} or WF_V approximately are parallel river systems, having more tributaries converging separately to catchment outlets than other catchments.

For the 13,456 catchments across TP, the proportion of catchments with a specific width function type are 22.58% (WF_I), 23.53% (WF_{II}), 25.27% (WF_{III}), 16.61% (WF_{IV}) and 12.02% (WF_V) respectively. As shown in Figure 6, however, there is no clear spatial pattern of the width function across the TP. The spatial distribution characteristics of the width function are relatively random, and the obvious spatial aggregation characteristics of different classification width functions cannot be found in our dataset.

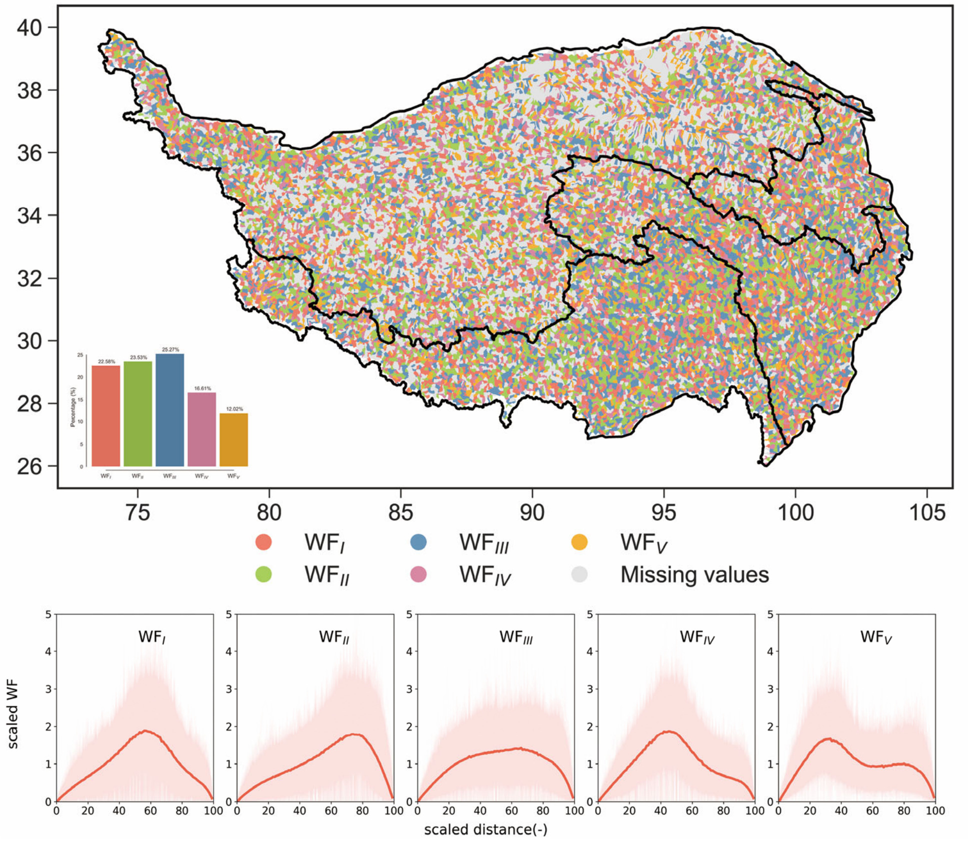

Figure 6 Typical width functions (bottom) and their spatial distribution across the Tibetan Plateau (top). At the bottom, the pink background indicates ranges of width function from the catchments subset of that type, while the red curve represents the median of the corresponding catchment subset.

4.3 WFIUH of catchments across the Tibetan Plateau

Based on the catchments' width function, instantaneous unit hydrographs for each of the 13,456 catchments across the TP are derived and presented in the TPHGD dataset, together with flow velocity estimated by Manning's approach for each grid cell. The time interval of the derived WFIUH is 30 minutes. There are some catchments located in the eastern Continental basin whose WFIUH cannot be extracted due to large irrigation areas and canals. Herein, characteristics of the WFIUH indicated by peak flow magnitude (Qp), time to peak (Tp) and concentration time (Tc, i.e., width of time base in WFIUH) for catchments across the TP are investigated. Their relationships with the 18 geomorphic metrics are also examined. The box plot of the relative magnitude of peak flow, time to peak, and the total width of the WFIUH and the spatial pattern of the three variables is demonstrated in Figure 7. This information can reveal the distribution features of the WFIUH of 13456 catchments in the Tibetan Plateau, which may be valuable for flood risk decision-making and management in this region.

As shown in Figure 7, the relative magnitude of peak flow for most catchments ranges from 0.05 to 0.15, with mean and median are 0.121 and 0.103 respectively. The smaller relative magnitude of the peak flow value represents a more uniform hydrograph distribution and a less obvious peak. The higher the Qp, the more susceptible the catchment is to flash floods. Catchments with a higher Qp are found in the northwest or north edge of the Inland Region (IR). Catchments in central IR have relatively lower Qp due to their smaller slopes. Catchments in the upper Yellow River Basin (YLRB) and Yangtze River Basin (YZRB) have correspondingly smaller Qp than catchments in lower YLRB and YZRB. Catchments in the Southwest Basin (SWB) have the highest Qp as compared to catchments in the other three regions. Particularly, in Nu River, Jinsha River, Lancang River, and the Palong Zangbo area, Qp can reach 0.2 and above, which explains well the high flood risks in those regions. In the middle and lower reaches of the Yarlung Zangbo River and the Shiquan River area, the relative magnitude of peak flow is also higher than that of the whole Tibetan Plateau.

The time to peak time in most catchments mainly ranges from 2h to 15 h, with mean and median Tp around 10.3h and 9.0h respectively. The spatial distribution of Tp across the Tibetan Plateau is similar to that of Qp, suggesting the shorter the Tp, the higher the Qp is. Catchment concentration time however varies from 10h-35h, with mean and median Tc around 18.3h and 16.5h respectively. Catchments with longer Tc are found in the central TP and YLRB. Catchments in the northwest IR, middle and lower reaches of the Yarlung Zangbo River, Palong Zangbo River and the Nu-Jinsha-Lancang basins all have relatively short Tc (<20h). For those regions with high Qp, short Tp and Tc, it is mainly because the catchments there tend to elongate and with a pinnate river network, higher slope and lower roughness.

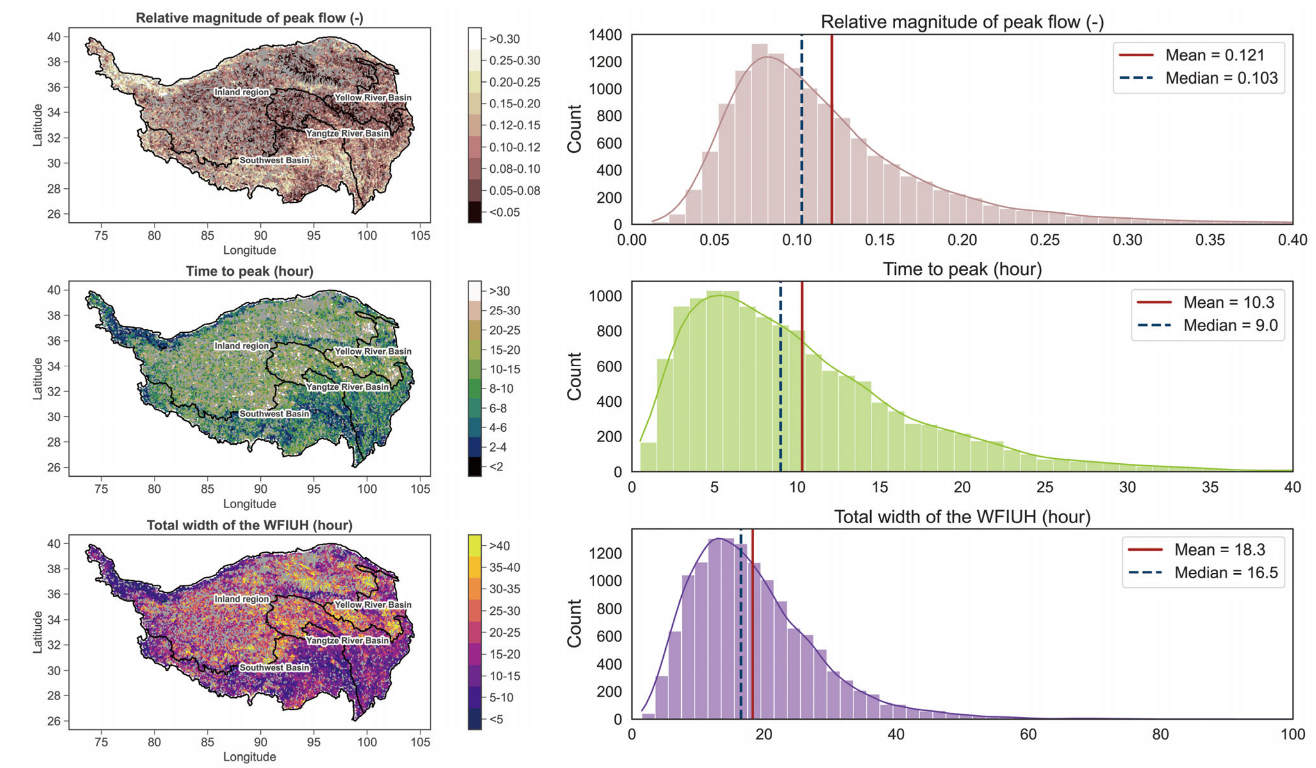

Figure 7 Distribution of WFIUH characteristics across the Tibetan Plateau. Left: spatial distribution; right: statistical distribution represented by histogram.

Figure 8 further shows the relationships of Qp, Tp and Tc against the 18 hydrogeomorphic metrics in our TPHGD dataset. It is found that Qp is positively related to slope, horizontal curvature and absolute vertical curvature. Qp is negatively related to catchment area, perimeter, length and circularity. The relationships of Tp against the hydrogeomorphic metrics are similar to those of Qp but in an oppositive direction. This suggests that a catchment with a larger, more circular shape may exhibit a more gradual rising limb in its hydrograph. Tc has a strong negative correlation with catchment slope as a steeper land surface can result in faster flow hence shortening the travelling time of water flow. Unsurprisingly, Tc is positively related to catchment size defined by area, perimeter and length.

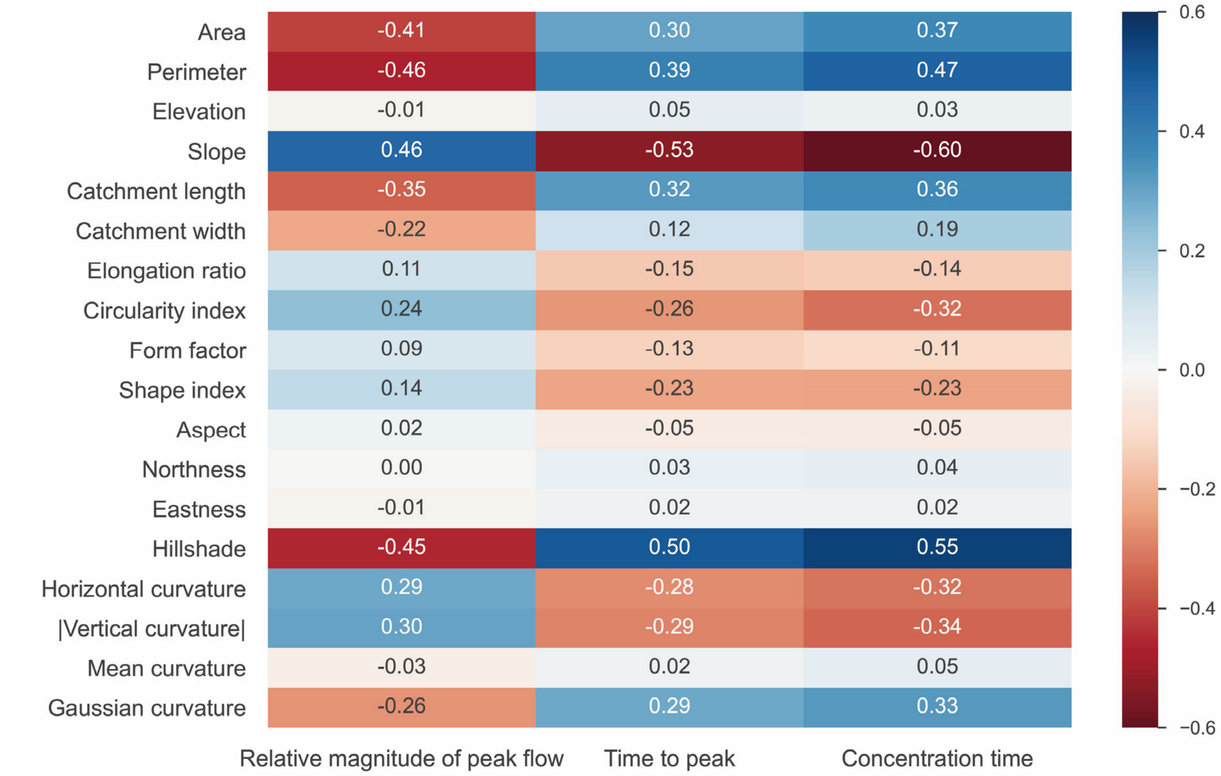

Figure 8 Correlations between WFIUH characteristics against 18 hydrogeomorphic metrics

4.4 Validity and uncertainty of derived WFIUH

The derived WFIUH in our TPHGD dataset is expected to represent the hydrological response function in a catchment, particularly contributing to generating a hydrograph of ungauged catchments in the Tibetan Plateau. To examine the validity, we have incorporated the derived WFIUH into a conceptual hydrological model GR4H (Perrin et al., 2003). The GR4H is a model with four parameters running at an hourly time step. The fourth parameter of GR4H (x4) represents the time base of a hypothetical unit hydrograph. In this study, the hypothetical unit hydrograph is replaced by our derived WFIUH, and the parameter x4 is then removed. The model was tested at four gauged catchments in the Tibetan Plateau for 48 flash flood events from 2008 to 2016. The required inputs of the model (rainfall and potential evapotranspiration) and the observed hourly streamflow data are obtained from China's Annual Hydrological Report.

Overall, the model performs well for most of the flash flood events as evaluated by NSE (Nash and Sutcliffe, 1970), bias in peak flow (BS_{qp}) and bias in time to peak (BS_{tp}) respectively (Figure 9). The simulated hydrograph is compared to the observed one for selected catchments and is shown in Figure 9 as well. As shown in Figure 9, the median NSE of the 48 flash events is around 0.67, for more than 50% of the 48 flash flood events with an absolute value of BS_{qp} lower than 10% and an absolute value of BS_{tp} lower than 3h. Peak flows of 26 flood events are underestimated while that of the other 22 events are overestimated, suggesting no systematic tendency in the modelling. The time to peak (T_p) of about two-thirds of simulated flood events lags behind the observed one, indicating uncertainties in the simulations.

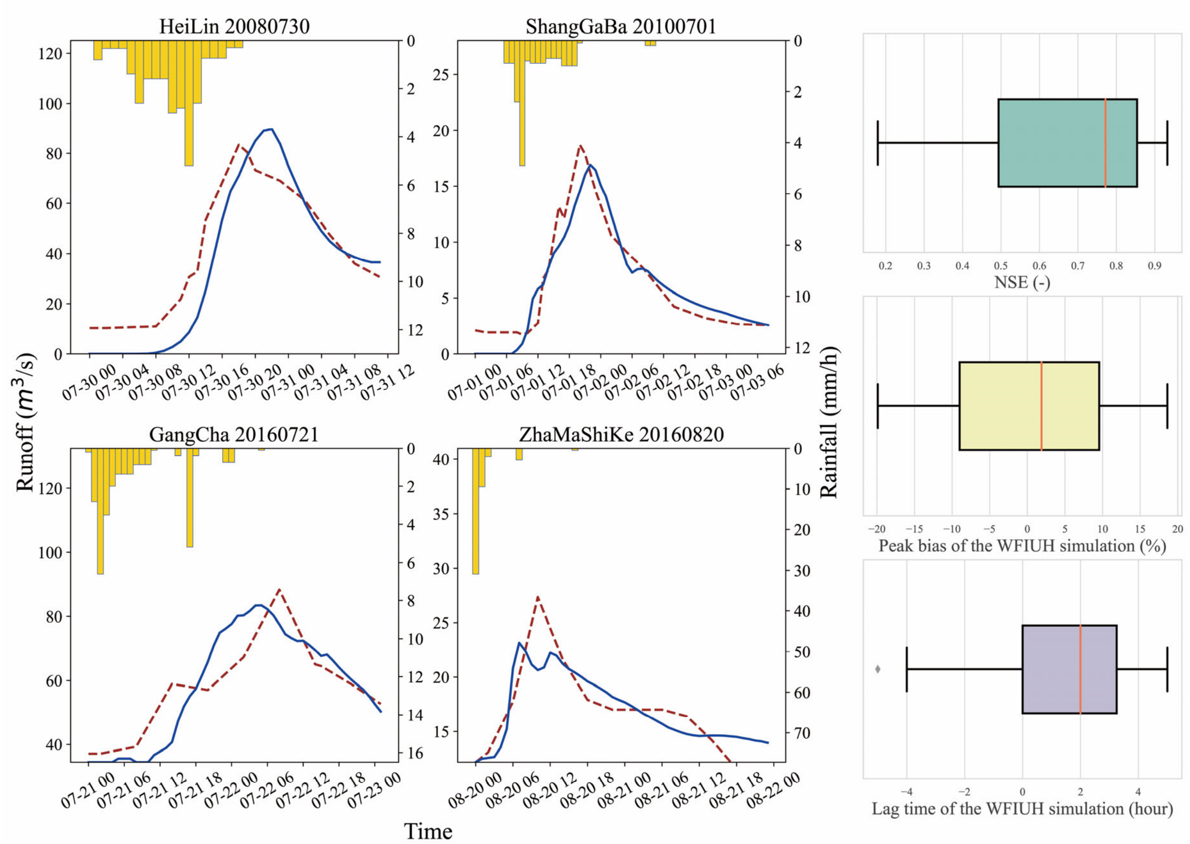

Figure 9 Performance of hydrological modeling by incorporating WFIUH into GR4H model. Left: comparison between simulated and observed hydrograph for flash events at different catchments (red-dashed curve is observed, blue-solid curve is simulated); Right, summary of overall model performance for 48 simulated flash flood events.

Uncertainties of the simulation can not only be due to the uncertainties in the derived WFIUH but also due to uncertainties in model structure, model inputs and model parameters. In terms of WFIUH, its validity could be affected by the spatial resolution and sources of DEM and the effectiveness of the method in estimating flow velocity. In this study, the DEM dataset from SRTM is used, which has with spatial resolution of 90m. We find it challenging to derive WFIUH for catchments with relatively small areas and with highly complicated topography by using the DEM from SRTM. Hence, DEM with higher spatial resolution can be conducive to improving the derivation of WFIUG for those catchments. It is worth noting that the uncertainties in WFIUH could be considerably affected by the estimate of flow velocity. In this study, Manning's approach is used to calculate flow velocity at each grid cell and then works with the catchment's width function to derive the WFIUH. Other approaches such as the Darcy–Weisbach formula (Katz et al., 1995), the Soil Conservation Service (SCS) formula (Haan et al., 1994), and the Maidment et al. (1996) uniform flow equation may result in a different estimate of flow velocity and hence the subsequent WFIUH. In addition, the roughness coefficient in Manning's approach assigned for each grid cell is affected by the accuracy of the land cover map, leading to uncertainties in the estimated flow velocity. It has been reported that a higher deviation in the roughness coefficient could result in a higher deviation of the hydrograph peaks (Kalyanapu et al., 2009). Thus, a detailed evaluation of Manning's roughness in different land cover types using remote sensing skills is needed to reduce the uncertainties (Mtamba et al., 2015; Sadeh et al., 2018). For further exploration of the uncertainties in the future, therefore in this version of the dataset, we provide also the width function for each catchment, which facilitates deriving WFIUH given different estimates of flow velocity.

5 Data and code availability

Our TPHGD dataset provides 18 hydrogeomorphic metrics for 18440 catchments across the Tibetan Plateau, together with width function and WFIUH of 13456 out of the 18440 catchments. Table 2 lists the structure of the dataset and the formats of the files there. The 18 metrics of all catchments are presented in an Excel file. The catchment's width function is stored in two separate CSV files, one of which represents the distance to the catchment outlet (i.e., x-axis in the WF plot) while the other represents the number of cells (equivalent to counts representing y-axis in the WF plot) at a given distance to the outlet. The gridded flow velocity map is presented as a tif file in Manning_velocity_map. Similar to the catchment's WF, WFIUH for each catchment is presented in two paired CSV files, WFIUH_flowtime.csv and WFIUH_cells.csv. The former provides flow time at a specific distance to the catchment outlet (i.e., the x-axis in the WFIUH plot), while the latter provides the number of cells (equivalent to counts and representing the y-axis in the WFIUH plot) within the corresponding distance. The dataset is archived and openly accessible via the Zenodo portal: https://doi.org/10.5281/zenodo.8280786 (Guo and Zheng, 2023).

The Python scripts in deriving WFIUH, curve fitting, and classification are freely available at https://github.com/YuhanGuo-22/Hydro_WFIUH_Classifier_and_Curve_fitting.git (last access: 18 Oct 2023). The dependency Python package (pysheds) used in deriving catchment WF is available at https://github.com/mdbartos/pysheds.

Table 2 Files in the TPHGD dataset

File names	Formats	Descriptions
1-Hydro_geomorphic_attribute	.xlsx 18440× 26	

		Hydrogeomophic metrics of 18440 catchments. Each row represents one catchment. Each column represents one metric (see Table 1).
2-WF_distance	.csv 13456 columns	Catchments' width function: distance to outlet (WF's x-axis). The first row is the catchment ID. Each column represents the distance to the catchment outlet for a catchment.
2-WF_cells.csv	.csv 13456 columns	Catchments' width function: cells/area (WF's y-axis). The first row is the catchment ID. Each column represents cells between a specific distance and an outlet for a catchment.
3-Manning_velocity_map	.tif (90m resolution)	Gridded flow velocity was calculated by Manning's approach. The value of each grid represents the mean velocity along the shortest flow path to the outlet.
4-WFIUH_flowTime.csv	.csv 13456 columns	Catchments' WFIUH: flow time to the outlet (WFIUH's x-axis). The first row is the catchment ID. Each column represents flow time to the outlet for a catchment.
4-WFIUH_cells.csv	.csv 13456 columns	Catchments' WFIUH: cells/area to outlet corresponding to a specific flow time (WFIUH's y-axis). The first row is the catchment ID. Each column represents the number of cells with a specific flow time to the outlet of a catchment.

6 Conclusions

The Tibetan Plateau provides an ideal setting for investigating the hydrological and geomorphic interactions between hydrological and geomorphic processes in a largely pristine natural environment, minimally impacted by human activities. The hydrological behaviours of catchments across the Tibetan Plateau however remain largely unknown due to its challenging physical conditions and data limitations. This study presents the inaugural version of a hydrogeomorphic dataset encompassing 18,440 catchments across the region. The dataset comprises 18 hydrogeomorphic metrics, particularly along with the width function and width function-based instantaneous unit hydrograph of each catchment. It can contribute to advancing our understanding of catchment hydrological behaviors in the Tibetan Plateau and hence improving water resources management and disaster mitigation in the region and its downstream. Particularly, the newly derived WFIUH can be conducive to flash flood modeling in catchments with little hydrological observations.

According to the dataset provided, it is found that catchments with higher elevation are in the western and central parts of the TP, while catchments in the western and southeast TP are steeper than other catchments in the TP. Catchments in central TP are more elongated with the pinnate river network, and catchments in western and eastern TP are less elongated and more fan-shaped. A power relationship (i.e., Hack's law) exists between catchments' area and length. We also find that the peak flow of WFIUH is positively related to slope and curvature but negatively related to catchment area, perimeter, length and circularity. The relationships of time-to-peak against the hydrogeomorphic metrics are similar to those of peak flow but in an oppositive direction. Catchment concentration time shows a positive relationship with catchment size but a strong negative correlation with catchment slope as a steeper land surface can result in faster flow hence shortening the travelling time of water flow.

The validity of the derived WFIUH has been confirmed by its successful integration into an hourly hydrological model for simulating flash flood events. Uncertainties in the simulation may arise from factors such as model structure, model inputs, model parameterization, and the derived WFIUH. Particularly, uncertainties in the WFIUH can be attributed to the resolution of DEM and the methods employed for calculating flow velocity. These aspects warrant further exploration in future research endeavors.

Author contributions.

HZ, YS, YYand YG conceived the research. YG and HZ developed the approaches and datasets. YY and YS checked the results. YG and HZ wrote the original draft. YY, YS and CW revised the draft.

Competing interests.

The contact author has declared that none of the authors has any competing interests.

References

Babar, M.: Hydrogeomorphology: fundamentals, applications and techniques, 2005.

Bhaskar, N. R., Parida, B. P., and Nayak, A. K.: Flood estimation for ungauged catchments using the GIUH, Journal of water resources planning management, 123, 228-238, 1997.

Botter, G. and Rinaldo, A.: Scale effect on geomorphologic and kinematic dispersion, Water Resources Research, 39, 2003.

Esper Angillieri, M. Y.: Morphometric analysis of Colangüil river basin and flash flood hazard, San Juan, Argentina, Environmental geology, 55, 107-111, 2008.

Florinsky, I.: Digital terrain analysis in soil science and geology, Academic Press2016.

Franchini, M. and O'Connell, P. E.: An analysis of the dynamic component of the geomorphologic instantaneous unit hydrograph, Journal of Hydrology, 175, 407-428, 1996.

Franchini, M. and Oconnell, P. E.: An analysis of the dynamic component of the geomorphologic instantaneous unit hydrograph, Journal of Hydrology, 175, 407-428, 10.1016/s0022-1694(96)80018-7, 1996.

Ge, J., You, Q., and Zhang, Y.: Effect of Tibetan Plateau heating on summer extreme precipitation in eastern China, Atmospheric Research, 218, 364-371, 2019.

Grimaldi, S., Petroselli, A., Alonso, G., and Nardi, F.: Flow time estimation with spatially variable hillslope velocity in ungauged basins, Advances in Water Resources, 33, 1216-1223, 10.1016/j.advwatres.2010.06.003, 2010.

Guo, Y. and Zheng, H.: Hydro-geomorphic unit hydrograph dataset of catchments across the Tibetan Plateau, Zenodo [data set], https://doi.org/10.5281/zenodo.8280786, 2023.

Gupta, V. K. and Waymire, E.: On the formulation of an analytical approach to hydrologic response and similarity at the basin scale, Journal of Hydrology, 65, 95-123, 1983.

Gupta, V. K., Waymire, E., and Wang, C.: A representation of an instantaneous unit hydrograph from geomorphology, Water resources research, 16, 855-862, 1980.

Haan, C. T., Barfield, B. J., and Hayes, J. C.: Design hydrology and sedimentology for small catchments, Elsevier1994.

Horton, R. E.: Erosional development of streams and their drainage basins-Hydrophysical approach to quantitative morphology, Bull. G. S. A, 56, 1945.

Jain, S., Singh, R., and Seth, S.: Design flood estimation using GIS supported GIUHApproach, Water resources management, 14, 369-376, 2000.

Jenson, S. K.: Applications of hydrologic information automatically extracted from digital elevation models, Hydrol. Process., 5, 31-44, 1991.

Kalyanapu, A. J., Burian, S. J., and McPherson, T. N.: Effect of land use-based surface roughness on hydrologic model output, Journal of Spatial Hydrology, 9, 2009.

Kang, S., Xu, Y., You, Q., Flügel, W.-A., Pepin, N., and Yao, T.: Review of climate and cryospheric change in the Tibetan Plateau, Environmental research letters, 5, 015101, 2010.

Katz, D. M., Watts, F. J., and Burroughs, E. R.: Effects of surface roughness and rainfall impact on overland flow, Journal of Hydraulic Engineering, 121, 546-553, 1995.

Kirkby, M.: Tests of the random network model, and its application to basin hydrology, Earth Surface Processes, 1, 197-212, 1976.

Kirshen, D. M. and Bras, R. L.: The linear channel and its effect on the geomorphologic IUH, Journal of Hydrology, 65, 175-208, 1983.

Koenderink, J. J. and Van Doorn, A. J.: Surface shape and curvature scales, Image vision computing, 10, 557-564, 1992.

Kumar, R., Chatterjee, C., Singh, R., Lohani, A., and Kumar, S.: Runoff estimation for an ungauged catchment using geomorphological instantaneous unit hydrograph (GIUH) models, Hydrological Processes: An International Journal, 21, 1829-1840, 2007.

Lehner, B., Verdin, K., and Jarvis, A.: New Global Hydrography Derived From Spaceborne Elevation Data, Eos, Transactions American Geophysical Union, 89, 93, 10.1029/2008eo100001, 2008.

Li, X., Long, D., Scanlon, B. R., Mann, M. E., Li, X., Tian, F., Sun, Z., and Wang, G.: Climate change threatens terrestrial water storage over the Tibetan Plateau, Nature Climate Change, 12, 801-807, 10.1038/s41558-022-01443-0, 2022.

Lindersson, S., Brandimarte, L., Mård, J., and Di Baldassarre, G.: Global riverine flood risk–how do hydrogeomorphic floodplain maps compare to flood hazard maps?, Natural hazards earth system sciences, 21, 2921-2948, 2021.

Maidment, D., Olivera, F., Calver, A., Eatherall, A., and Fraczek, W.: Unit hydrograph derived from a spatially distributed velocity field, Hydrol. Process., 10, 831-844, 1996.

Mesa, O. J. and Mifflin, E. R.: On the relative role of hillslope and network geometry in hydrologic response, in: Scale problems in hydrology, Springer, 1-17, 1986.

Mölg, T., Maussion, F., and Scherer, D.: Mid-latitude westerlies as a driver of glacier variability in monsoonal High Asia, Nature Climate Change, 4, 68-73, 10.1038/nclimate2055, 2014.

Moussa, R.: What controls the width function shape, and can it be used for channel network comparison and regionalization?, Water Resources Research, 44, 19, 10.1029/2007wr006118, 2008.

Mtamba, J., Van Der Velde, R., Ndomba, P., Zoltán, V., and Mtalo, F.: Use of Radarsat-2 and Landsat TM Images for Spatial Parameterization of Manning's Roughness Coefficient in Hydraulic Modeling, Remote Sensing, 7, 836-864, 10.3390/rs70100836, 2015.

NADEN, P. S.: Spatial variability in flood estimation for large catchments: the exploitation of channel network structure, Hydrological Sciences Journal, 37, 53-71, 1992.

Nash, J. E. and Sutcliffe, J. V.: River flow forecasting through conceptual models part I—A discussion of principles, Journal of Hydrology, 10, 282-290, 1970.

Nasri, S., Cudennec, C., Albergel, J., and Berndtsson, R.: Use of a geomorphological transfer function to model design floods in small hillside catchments in semiarid Tunisia, Journal of hydrology, 287, 197-213, 2004.

Nowicka, B. and Soczynska, U.: Application of GIUH and dimensionless hydrograph models in ungauged basins, FRIENDS in Hydrology, 187, 197-203, 1989.

Passalacqua, P., Tarolli, P., and Foufoula-Georgiou, E.: Testing space-scale methodologies for automatic geomorphic feature extraction from lidar in a complex mountainous landscape, Water resources research, 46, 2010.

Peng Gong, Han Liu, Meinan Zhang, Li, C., Wang, J., and Huang, H.: Stable classification with limited sample: Transferring a 30-m resolution sample set collected in 2015 to mapping 10-m resolution global land cover in 2017, Sci. Bull, 64, 370-373, 2019.

Perrin, C., Michel, C., and Andréassian, V.: Improvement of a parsimonious model for streamflow simulation, Journal of hydrology, 279, 275-289, 2003.

Prusevich, A., Lammers, R., and Glidden, S.: MERIT-Plus Dataset: Delineation of endorheic basins in 5 and 15 min upscaled river networks, MultiSector Dynamics-Living, Intuitive, Value-adding, Environment, 2022.

Rigon, R., Rodriguez-Iturbe, I., Maritan, A., Giacometti, A., Tarboton, D. G., and Rinaldo, A.: On Hack's Law, Water Resources Research, 32, 3367-3374, 10.1029/96wr02397, 1996.

Rinaldo, A., Marani, A., and Rigon, R.: Geomorphological dispersion, Water Resources Research, 27, 513-525, 1991.

Rinaldo, A., Vogel, G. K., Rigon, R., and Rodriguez-Iturbe, I.: Can one gauge the shape of a basin, Water Resources Research, 31, 1119-1127, 10.1029/94wr03290, 1995.

Rodríguez-Iturbe, I. and Valdes, J. B.: The geomorphologic structure of hydrologic response, Water resources research, 15, 1409-1420, 1979.

Rodríguez-Iturbe, I. and Valdés, J. B.: The geomorphologic structure of hydrologic response, Water resources research, 15, 1409-1420, 1979.

Saco, P. M. and Kumar, P.: Kinematic dispersion effects of hillslope velocities, Water Resources Research, 40, n/a-n/a, 10.1029/2003wr002024, 2004.

Sadeh, Y., Cohen, H., Maman, S., and Blumberg, D.: Evaluation of Manning's n Roughness Coefficient in Arid Environments by Using SAR Backscatter, Remote Sensing, 10, 1505, 10.3390/rs10101505, 2018.

Safanelli, J., Poppiel, R., Ruiz, L., Bonfatti, B., Mello, F., Rizzo, R., and Demattê, J.: Terrain Analysis in Google Earth Engine: A Method Adapted for High-Performance Global-Scale Analysis, ISPRS International Journal of Geo-Information, 9, 400, 10.3390/ijgi9060400, 2020.

Sassolas-Serrayet, T., Cattin, R., and Ferry, M.: The shape of watersheds, Nature Communications, 9, 10.1038/s41467-018-06210-4, 2018.

Scheidegger, A. E.: Hydrogeomorphology, Journal of Hydrology, 20, 193-215, 1973.

Sidle, R. C. and Onda, Y.: Hydrogeomorphology: overview of an emerging science, Hydrol. Process., 18, 597-602, 2004.

Singh, P., Mishra, S., and Jain, M.: A review of the synthetic unit hydrograph: from the empirical UH to advanced geomorphological methods, Hydrological Sciences Journal, 59, 239-261, 2014.

Strahler, A. N.: Quantitative analysis of watershed geomorphology, Eos, Transactions American Geophysical Union, 38, 913-920, 1957.

Troutman, B. M. and Karlinger, M. R.: Unit hydrograph approximations assuming linear flow through topologically random channel networks, Water Resources Research, 21, 743-754, 10.1029/wr021i005p00743, 1985.

Yang, L., Ma, J., Wang, X., and Tian, F.: Hydroclimatology and Hydrometeorology of Flooding Over the Eastern Tibetan Plateau, Journal of Geophysical Research: Atmospheres, 127, e2022JD037097, 2022.

Yao, T., Thompson, L., Yang, W., Yu, W., Gao, Y., Guo, X., Yang, X., Duan, K., Zhao, H., Xu, B., Pu, J., Lu, A., Xiang, Y., Kattel, D. B., and Joswiak, D.: Different glacier status with atmospheric circulations in Tibetan Plateau and surroundings, Nature Climate Change, 2, 663-667, 10.1038/nclimate1580, 2012.

Yao, T., Bolch, T., Chen, D., Gao, J., Immerzeel, W., Piao, S., Su, F., Thompson, L., Wada, Y., Wang, L., Wang, T., Wu, G., Xu, B., Yang, W., Zhang, G., and Zhao, P.: The imbalance of the Asian water tower, Nature Reviews Earth & Environment, 10.1038/s43017-022-00299-4, 2022.